ADVANCED MATERIALS
www.advmat.de

Activatable Graphene Quantum-Dot-Based Nanotransformers for Long-Period Tumor Imaging and Repeated Photodynamic Therapy

Yuqi Yang, Baolong Wang, Xu Zhang, Hongchuang Li, Sen Yue, Yifan Zhang, Yunhuang Yang, Maili Liu, Chaohui Ye, Peng Huang, and Xin Zhou**

Photodynamic therapy (PDT) is considered as an emerging therapeutic modality against cancer with high spatiotemporal selectivity because the utilized photosensitizers (PSs) are only active and toxic upon light irradiation. To maximize its effectiveness, PDT is usually applied repetitively for ablating various tumors. However, the total overdose of PSs from repeated administrations causes severe side effects. Herein, acidity-activated graphene quantum dots-based nanotransformers (GQD NT) are developed as PS vehicles for long-period tumor imaging and repeated PDT. Under the guidance of Arg-Gly-Asp peptide, GQD NT targets to tumor tissues actively, and then loosens and enlarges in tumor acidity, thus promising long tumor retention. Afterwards, GQD NT transforms into small pieces for better penetration in tumor. Upon laser irradiation, GQD NT generates mild hyperthermia that enhances cell membrane permeability and further promotes the PSs uptake. Most intriguingly, the as-prepared GQD NT not only "turns-on" fluorescence/magnetic resonance signals, but also achieves efficient repeated PDT. Notably, the total PSs dose is reduced to 3.5 μmol kg^{-1}, which is 10–30 times lower than that of other reported works. Overall, this study exploits a smart vehicle to enhance accumulation, retention, and release of PSs in tumors through programmed deformation, thus overcoming the overdose obstacle in repeated PDT.

1. Introduction

Cancer is one of the leading causes of human death worldwide. Some clinical imaging and treatment approaches that have been employed to date suffer from low efficiency due to nonspecific drug distribution, rapid drug clearance, drug resistance, or high toxicity to normal tissues. Fortunately, the application of nanotechnology has greatly improved tumor imaging contrast and anticancer treatment efficacy.[1] Traditionally, nanomaterials have been used as carriers that can load diagnostic or therapeutic agents and deliver them to target areas.[2] The bioactivity of loaded therapeutic agents, e.g., microRNA,[3] DNA,[4] and proteins,[5] is retained because the relatively stable microenvironment provided by nanocarriers can prevent the denaturation or degradation of payloads in the bloodstream. As a consequence of the enhanced permeability and retention (EPR) effect,[6] nanomedicine is able to passively accumulate in tumor tissues, which markedly decreases the

Y. Yang, B. Wang, X. Zhang, H. Li, S. Yue, Y. Yang, M. Liu, C. Ye, X. Zhou
Key Laboratory of Magnetic Resonance in Biological Systems
State Key Laboratory of Magnetic Resonance and Atomic and Molecular Physics
National Center for Magnetic Resonance in Wuhan
Wuhan Institute of Physics and Mathematics
Innovation Academy for Precision Measurement Science and Technology
Chinese Academy of Sciences – Wuhan National Laboratory for Optoelectronics
Huazhong University of Science and Technology
Wuhan 430071, China
E-mail: xinzhou@wipm.ac.cn

Y. Yang, B. Wang, X. Zhang, H. Li, S. Yue, Y. Yang, M. Liu, C. Ye, X. Zhou
Optics Valley Laboratory
Wuhan, Hubei 430073, China

Y. Yang, B. Wang, X. Zhang, H. Li, S. Yue, Y. Yang, M. Liu, C. Ye, X. Zhou
University of Chinese Academy of Sciences
Beijing 100049, China

Y. Zhang, P. Huang
Marshall Laboratory of Biomedical Engineering
International Cancer Center
Laboratory of Evolutionary Theranostics (LET)
School of Biomedical Engineering
Shenzhen University Medical School
Shenzhen University
Shenzhen, Guangdong 518055, China
E-mail: peng.huang@szu.edu.cn

The ORCID identification number(s) for the author(s) of this article can be found under https://doi.org/10.1002/adma.202211337

DOI: 10.1002/adma.202211337

in vivo clearance rate, increases the imaging period and prolongs the therapeutic action time. Moreover, nanomedicine decorated with specific ligands can further increase their targeting ability of tumors.[7] For example, Arg-Gly-Asp (RGD) peptide modified nanomedicines could recognize the $\alpha_v\beta_3$ integrin expressed in vascular endothelial cells and mediates penetration into tissues and cells.[8] The active targeting can further reduce the toxicity of therapeutic agents to normal tissues.[9]

Photodynamic therapy (PDT) is a developing clinical treatment modality that employs a specific light to irradiate and activate the localized photosensitizers (PSs). Then, the excited PS transfers energy to oxygen and produces reactive oxygen species (ROS), which reacts rapidly with cellular components to induce cancer cells apoptosis and necrosis.[10] The most attractive advantage of PDT is its low toxicity to nontarget areas, allowing repetitive injections at intervals to achieve an optimal treatment efficacy. However, repetitive injections in each PDT session easily lead to the overdose of PSs in the body. Although PSs are silent and nontoxic in the dark, the large amount of residual PSs in normal tissues may cause pain, fever and systemic side effects.[11] Moreover, the residual PSs can also be activated by sunlight. According to the clinical protocols, patients receiving PDT must wear protective clothing and sunglasses to avoid light for ≈6 weeks after treatment.[12] The lack of tumor selectivity and unfavorable biodistribution of PSs that cause this situation should be carefully considered and urgently improved by decreasing the total dose, minimizing side-effects and maintaining advantages of multiple-session PDT as a safe therapeutic modality.

Integration of photosensitizing moiety and targeting ability by combining PDT with nanotechnology provides a chance to overcome these difficulties. Previously, some PSs were used as building blocks to fabricate nanoparticles, such as porphyrin metal organic frameworks,[13] nanoporphyrin liposomes,[14] and single-component peptide depot.[15] Some PSs were directly loaded into nanocarriers through weak interactions, such as π–π interaction,[16] Vander Waals force,[17] and hydrogen bonds.[18] Among various nanocarriers, graphene and its derivatives have gained much attention as drug carriers due to their large specific surface area.[19] The characteristic sp^2-bonded carbon atoms in graphene allow drug molecules adsorption through π–π stacking interaction.[20] Moreover, the abundant hydrophilic hydroxyl, epoxide and carboxylic acid groups at the edges and defects of graphene nanosheets can form hydrogen bonds with drugs and provide active sites for covalent linkages.[21] Graphene quantum dots (GQD) are extremely small graphene nanosheets that owns all the above advantages. In addition, their fluorescence property and good biocompatibility make GQD an excellent vehicle for drug delivery.[22]

In this work, we designed a modular self-assembly approach to encapsulate PSs in GQD-based nanotransformers (GQD NT), which reduced the total dose by prolonging the retention time of PSs in tumor tissues. Small-sized GQD was transformed to larger GQD NT by easily mixing the following three modules (**Scheme 1**): 1) a loading module, which was mainly composed of GQD, offers large surface areas for PSs loading through π–π stacking interaction, hydrophilic–hydrophobic interaction, or hydrogen bonds; 2) a targeting module that consists of active molecules to target lesions; and 3) a linking module that links the abovementioned modules through host–guest interactions between β-cyclodextrin and adamantine.[23] The produced GQD NT not only served as the vehicle to deliver PSs to target areas like "Autobots," but also exhibited mild photothermal effect that increased the permeability of cell membrane and improved the cellular uptake of PSs. After successful transportation to tumor areas, the GQD NT would recognize the tumor acidity and loosen their tight structure. The slow loosening first expanded their diameter over 100 nm for better retention in tumor tissues, and then completely untied and released the loaded PSs. As a result, the loaded PSs could retain in tumor tissues for a long period, which provided an opportunity for repeated PDT. In vivo magnetic resonance and fluorescence duplex imaging results illustrated that the tumor area could be clearly distinguished from normal tissues after intravenous (i.v.) injection, and the loaded PSs sustained in tumor tissues for several days, which promising the repeated PDT. The designed GQD NT improved imaging properties and reduced the total dose of PSs, which provided a new solution to achieve the repeated PDT by enhancing tumor accumulation and prolonging tumor retention of PSs.

2. Results and Discussion

2.1. Synthesis and Characterization of the GQD NT

GQD NT were easily formed by self-assembly of the targeting module, loading module and linking module at room temperature, and drugs molecules were simultaneously encapsulated during the host–guest interaction process between β-cyclodextrin and adamantine (Scheme 1). A cyclic peptide, RGD, was selected as a targeting molecule to enhance the selectivity because of its high affinity to the $\alpha_v\beta_3$ integrin expressed in some tumor cells and vascular endothelial cells. The GQD and RGD were modified with the guest molecule adamantane via a single-stranded PEG bridge to form the loading module and targeting module, and 8-armed PEG was modified with the host molecule β-cyclodextrin to form the linking module (Figures S1–S8, Supporting Information). After the host–guest interaction between the targeting module, loading module and the linking module, the free GQD (**Figure 1**a) with an average diameter of 4 nm were self-assembled into GQD NT (Figure 1b) with a relatively uniform diameter of ≈60 nm (Figures S9 and S10, Supporting Information). The narrow size distribution indicated the good dispersity and negligible aggregation of GQD NT. X-ray photoelectron spectroscopy (XPS, Figure S11, Supporting Information) analysis and energy dispersive X-ray spectroscopy (EDS, Figure S12, Supporting Information) characterizations demonstrated the abundant presence of the C and O elements. Due to the photothermal effect of GQD, the GQD NT, which contained 42 wt% GQD, can achieve light-induced mild hyperthermia (Figure S13, Supporting Information). The temperature changes of GQD NT, TCPP@GQD NT, and Mn-TCPP@GQD NT solutions are similar under same condition of laser irradiation. According to the previous research, the mild hyperthermia could increase the permeability of cell membrane,[24] thus enhancing the cellular uptake of GQD NT.

When reaching tumor tissues, the GQD NT were able to transform into a loosen state and then completely dissociated over time. TEM images showed that the GQD NT sustained stable in physiological pH (Figure S14, Supporting Information). The acidic tumor extracellular pH (≈6.2) could trigger the

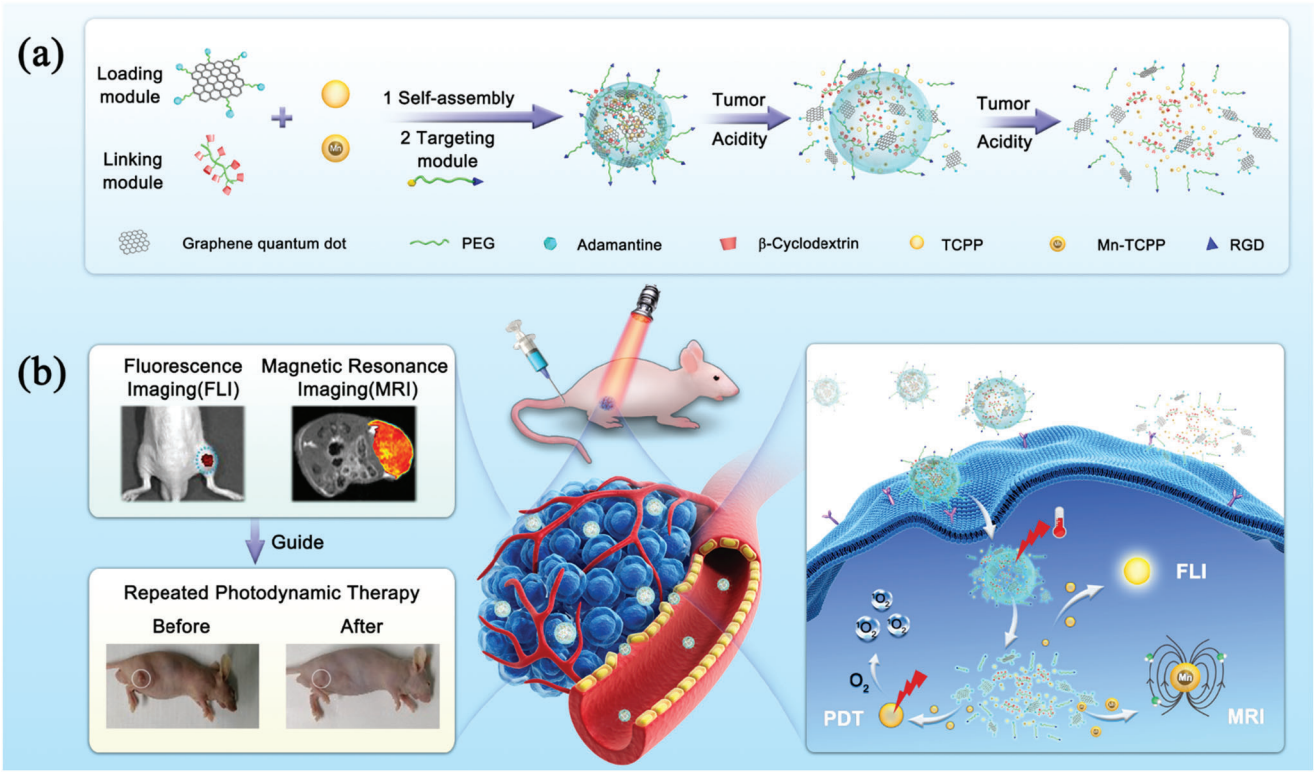

Scheme 1. A modularized self-assembly method to fabricate graphene quantum dots-based nanotransformers (GQD NT) for long period tumor imaging and repeated PDT. a) Photosensitizer (PS) tetracarboxylphenyl porphyrin (TCPP) and MRI contrast agent Mn-TCPP can be easily encapsulated into the GQD NT vehicle during the self-assembly process of the targeting, loading and linking modules. Tumor acidity will trigger GQD NT transformation and drugs release. b) The loaded PS molecules are transported to target areas under the guidance of surface RGD peptides. Then, GQD NT was transformed to the loose state in the acidic tumor microenvironment, which increased the diameter over 100 nm for longer retention in tumor tissues. The transformed GQD NT was further disassembled completely with the extended retaining time, resulting in the release of the encapsulated drugs, the recovery of FLI and MRI signals, and the "turned-on" repeated PDT.

transformation of tight GQD NT into a loosen state and increased their diameter over 100 nm (Figure 1c), which was favorable for long tumor retention. When time prolonged to 24 h, the GQD NT was dissociated, and the diameter decreased to 15 nm (Figure 1d,e). According to previous studies,[25] such a small size was beneficial to the efficient extravasation through tumor vascular fenestrations, deep penetration and easy incorporation of nanomedicine into cancer cells, thus further enhancing the uptake of PSs. The intracellular lysosome pH (≈5.2) induced faster transformation (Figure S14, Supporting Information), promoting the release of PSs from the un-transformed GQD NT. Size distribution changes further confirmed the deformation of GQD NT in acidic environment (Figure S15, Supporting Information).

2.2. Photosensitizers Loading by GQD NT

Owing to their large specific surface area and intrinsically polyaromatic structure, graphene-based materials are able to load a variety of drug molecules through π–π stacking. In this study, tetracarboxylphenyl porphyrin (TCPP) and Mn-TCPP were successfully encapsulated by GQD NT. As shown in Figure 1f, the zeta potential gradually changed from negative to positive during the process of PEG modification, self-assembly and drug encapsulation. UV–vis spectra of the obtained aqueous solutions showed typical peaks of TCPP and Mn-TCPP (Figure 1g), suggesting the successful loading of the hydrophobic drugs in GQD NT. Furthermore, the hydrodynamic size distribution did not show an obvious change after drug loading (Figure S16, Supporting Information). Compared with free GQD, the loading capacity of GQD NT increased by 215% and 249% for TCPP and Mn-TCPP respectively (Figure 1h). Additionally, the UV–vis and fluorescence spectra did not show significant change within 8 days of storage (Figure S17, Supporting Information), indicating the good stability of TCPP@GQD NT and Mn-TCPP@GQD NT.

Next, the optical and magnetic resonance properties of the encapsulated PSs were investigated. The fluorescence emission peaks of the TCPP@GQD NT were located at 655 and 720 nm upon excitation at 418 nm (Figure S18, Supporting Information). The Mn-TCPP loaded GQD NT exhibited concentration-dependent T_1-weighted MR contrast imaging property (Figure S19, Supporting Information). The longitudinal relaxivity value (r_1) of the Mn-TCPP@GQD NT was 12.65 mM^{-1} s^{-1} (Figure S19a,b, Supporting Information), which was 2–5 times higher than some traditional T_1 MRI contrast agents (Table S1, Supporting Information). The transverse relaxivity value (r_2) of the Mn-TCPP@GQD NT was 32.34 mM^{-1} s^{-1}, and no obvious contrast enhancement was observed in T_2-weighted MR images

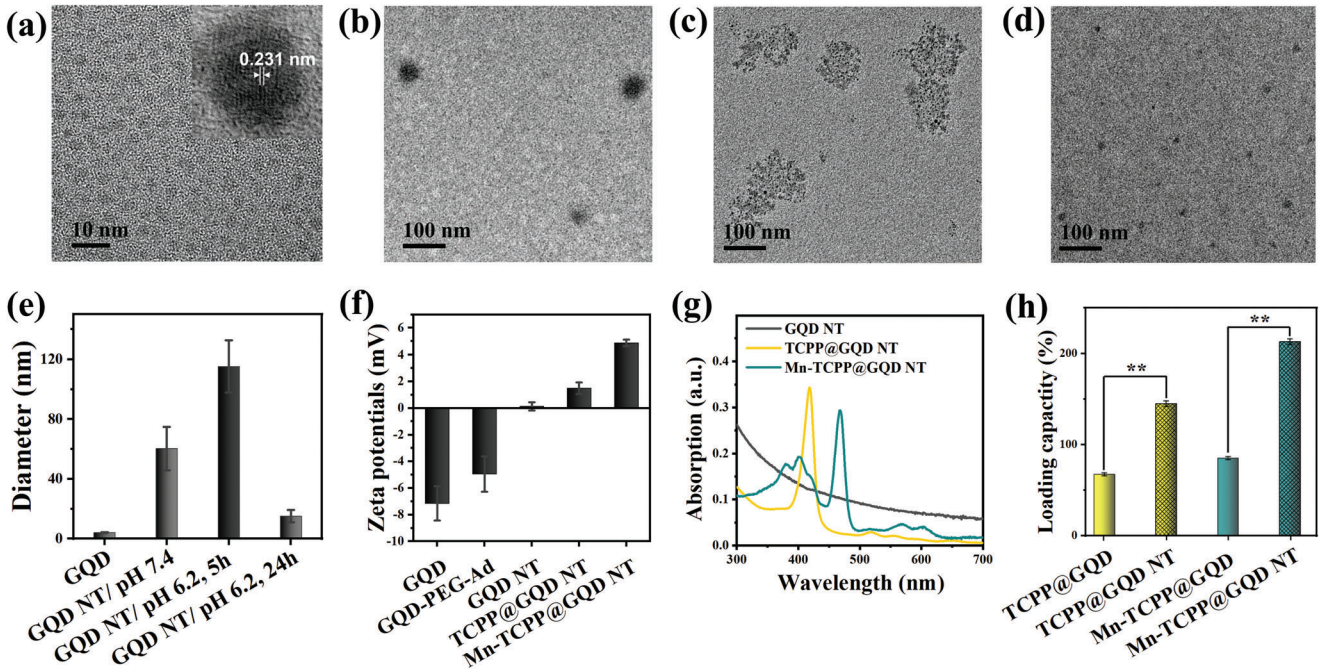

Figure 1. Characterization of GQD NT and their loading properties. Transmission electron microscopy (TEM) images of a) graphene quantum dots (GQD), b) graphene quantum dots-based nanotransformers (GQD NT), c) GQD NT in pH 6.2 for 5 h, d) GQD NT in pH 6.2 for 24 h, illustrating that tumor acidity triggered the looseness and dissociation of GQD NT. e) Diameter distribution counted by TEM images. f) Zeta potentials of GQD, GQD-PEG-adamantane (Ad), GQD NT, TCPP@GQD NT, and Mn-TCPP@GQD NT. g) UV–vis spectra indicated the successful encapsulation of TCPP and Mn-TCPP in GQD NT. h) Drug loading capacity of GQD and GQD NT (**$p < 0.01$).

(Figure S19c,d, Supporting Information). As the r_2/r_1 ratio was 2.56, the Mn-TCPP@GQD NT could potentially be used as a T_1 MRI contrast agent for in vivo application.

2.3. In Vitro Targeting PDT Effect of TCPP@GQD NT

Due to the RGD modification, the in vitro active targeting ability of TCPP@GQD NT was evaluated on different cell lines, such as integrin $\alpha_v\beta_3$-positive A549 cells, $\alpha_v\beta_3$-negative MCF7 and MRC5 cells. As shown in **Figure 2**a, the A549 cells exhibited intense fluorescence signals of TCPP in the cytoplasm, demonstrating that a large amount of TCPP@GQD NT accumulated in the cells. Weak fluorescence signal in MRC5 cells and MCF7 cells were observed, suggesting the low cellular uptake efficiency of TCPP@GQD NT on integrin $\alpha_v\beta_3$-negative cells. Moreover, when the integrin $\alpha_v\beta_3$ was blocked before TCPP@GQD NT incubation, the fluorescence (FL) intensity in A549 cells was much lower than that of noninhibited cells. Quantitative fluorescence analysis also demonstrated that the amount of TCPP in A549 cells was significantly higher than that in other cells lines (Figure 2b). 3D cell spheroid studies further demonstrated that the present of RGD on TCPP@GQD NT could improve the targeting ability of A549 cells (Figure S20–S22, Supporting Information).The above results confirmed the excellent targeting ability of TCPP@GQD NT toward $\alpha_v\beta_3$-positive cells. The fluorescence intensity in the laser irradiated area was 2.3 times higher than the unirradiated area (Figure S23, Supporting Information), demonstrating that mild hyperthermia could enhance cell uptake of TCPP@GQD NT.

To evaluate the tumor acidic microenvironment-triggered transformation of TCPP@GQD NT and the PSs release, A549 cells were incubated with TCPP@GQD NT at different pH values. As shown in Figure 2c,d, and Figure S24–S27 (Supporting Information), the enhanced yellow fluorescence signals indicated the increased amount of free TCPP, thus GQD NT released more TCPP in lower pH. The results were in agreement with that GQD NT transformed faster in lower pH and intended to become loosen to release more drugs.

Next, the in vitro PDT efficiency was evaluated. Under 650 nm laser irradiation, the TCPP@GQD NT showed a light dose-dependent cytotoxicity to A549 cells, and the average viability decreased to only 6.8% when the irradiation time prolonged to 10 min (Figure 2e). Then, cells were treated with GQD NT and TCPP@GQD NT respectively, followed by 10 min laser irradiation. Regardless of the presence of GQD NT, cellular viability maintained well under irradiation (Figure 2f), indicating favorable biocompatibility of the vehicle (Figure S28, Supporting Information) and negligible phototoxicity of the used laser dose. Meanwhile, a significant decrease in cellular viability was observed only after TCPP@GQD NT treatment and the following laser irradiation, because PDT was activated by PS under laser irradiation. To evaluate the PDT efficiency, 2′,7′-dichlorodihydrofluorescein diacetate (DCFH-DA) was introduced, as its green fluorescence is strongly enhanced upon reaction with ROS. As shown in Figure 2g, strong green fluorescence was observed only in TCPP@GQD NT-incubated and laser-irradiated A549 cells, indicating that efficient PDT produced a large amount of ROS that caused apoptosis of the target cells. All these results demonstrated the excellent

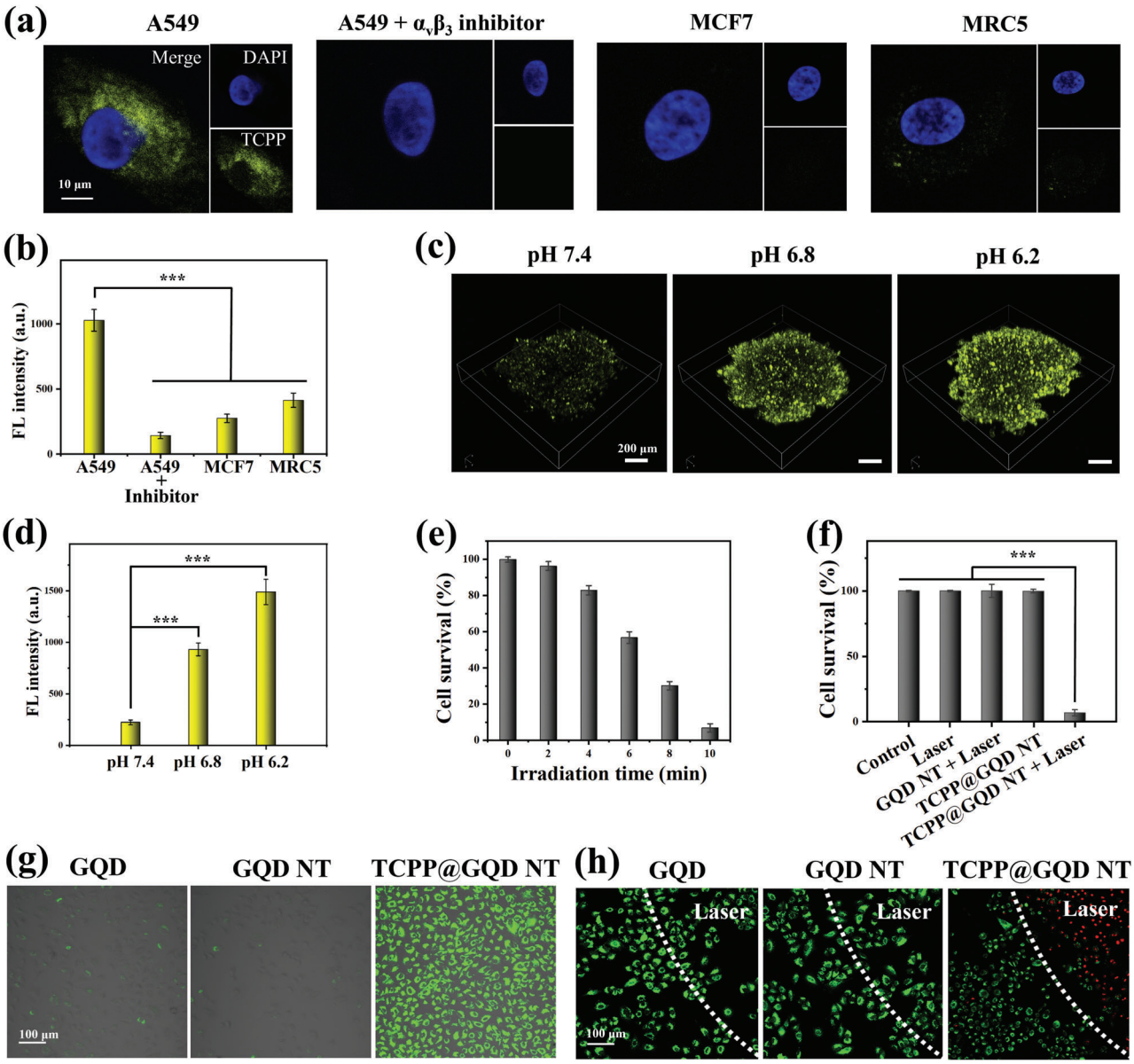

Figure 2. Selective transport of TCPP@GQD NT to $\alpha_v\beta_3$-positive A549 cells for efficient PDT. a) Selectivity of TCPP@GQD NT to $\alpha_v\beta_3$-positive cells. Cells were treated with 150 μg mL^{-1} TCPP@GQD NT for 1 h. The yellow fluorescence originated from the loaded TCPP. Scale bar, 10 μm. b) Quantitative analysis of the fluorescence (FL) intensity of TCPP@GQD NT in different cells (***$p < 0.001$). c) Acidity triggered the recovery of fluorescence signal from TCPP. 3D cell spheroids were incubated with 150 μg mL^{-1} TCPP@GQD NT in pH 6.2, 6.8, and 7.4 buffers, respectively. Scale bar, 200 μm. d) Quantitative analysis of the fluorescence intensity of TCPP in A549 cells at pH 7.4, 6.8, and 6.2. e) Viability of A549 cells that were treated with 150 μg mL^{-1} TCPP@GQD NT, followed by 650 nm laser irradiation for different times. f) Viability of A549 cells that were treated with GQD NT or TCPP@GQD NT, followed by 10 min laser irradiation. g) Imaging the intracellular singlet oxygen produced by GQD, GQD NT, and TCPP@GQD NT after laser irradiation, respectively. Scale bar, 100 μm. h) PDT-mediated tumor cell apoptosis. Live and dead cells were stained with calcein AM (green) and propidium iodide (PI, red), respectively. The areas in the white dotted lines were irradiated with 650 nm laser at a power density of 100 mW cm^{-2} for 10 min. Scale bar, 100 μm.

biocompatibility and high PDT efficiency of TCPP@GQD NT. Then, calcein AM (green) was introduced to label living cells, and propidium iodide (PI, red) was used to label dead cells. As shown in Figure 2h, the cells incubated with GQD and GQD NT showed high cell viability regardless of whether they were subjected to laser irradiation, indicating favorable biocompatibility. However, a large number of dead cells were observed in the laser-irradiated area in the cells incubated with TCPP@GQD NT. The Annexin V-flu647/PI apoptosis assay also confirmed that TCPP@GQD NT-induced PDT led to apoptosis of A549 cells (Figure S29, Supporting Information).

2.4. In Vivo Fluorescence and Magnetic Resonance Duplex Imaging of TCPP@GQD NT

To study the in vivo structural transformation, TCPP@GQD NT was injected to A549 tumor-bearing mice. Bio-TEM images of

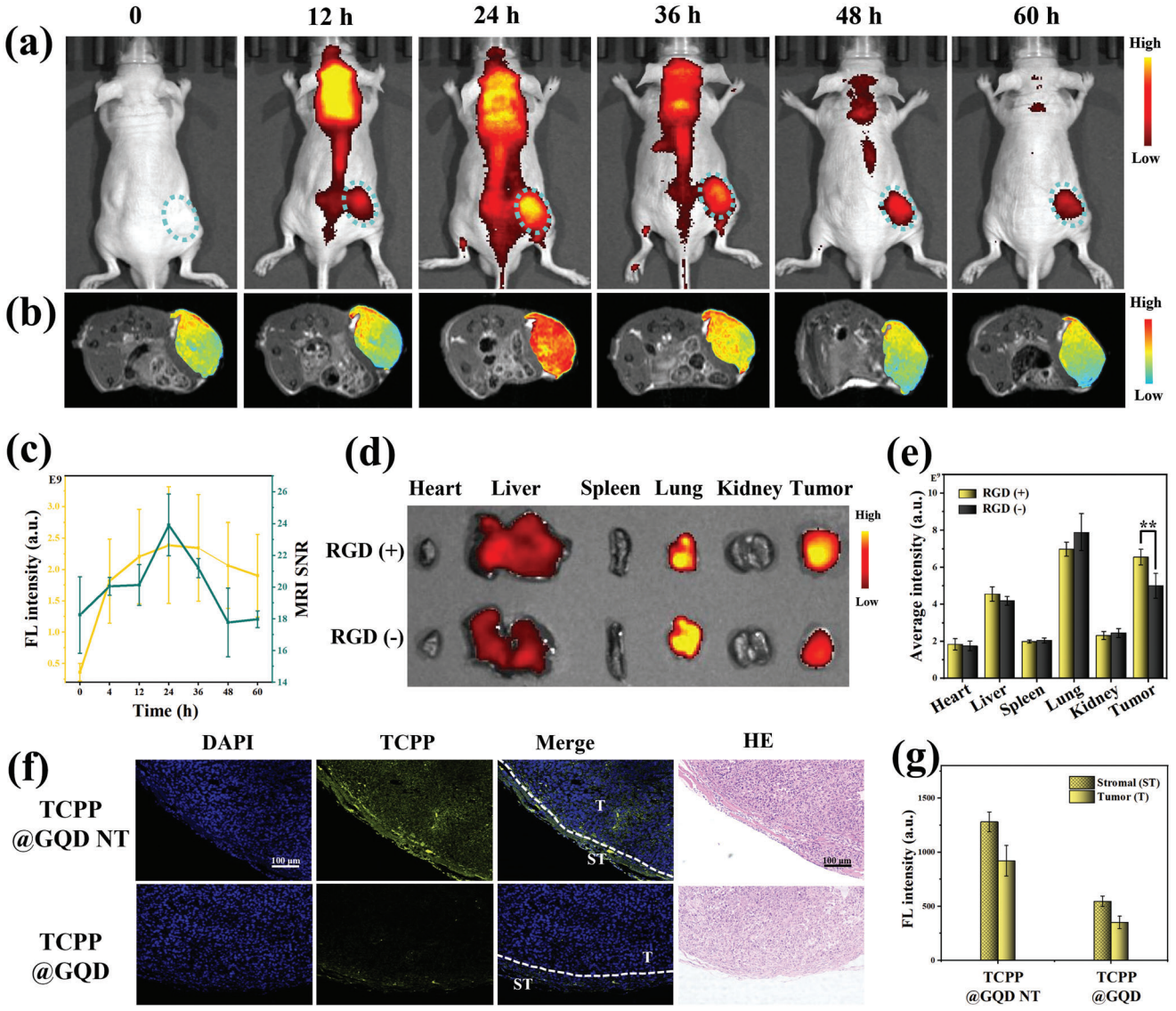

Figure 3. In vivo fluorescence imaging (FLI)/magnetic resonance imaging (MRI). a) In vivo FLI of A549 tumor-bearing mice after intravenous injection of TCPP@GQD NT. Tumor area is circled with blue dashed line. b) In vivo MR images of A549 tumor-bearing mice after intravenous injection of Mn-TCPP@GQD NT. c) Changes of fluorescence intensity (yellow) and MRI signal-noise ration (SNR, cyan) of tumors over time ($n = 3$). d) Ex vivo FLI and e) Fluorescence intensity measurements of major organs and tumor tissues from mice treated with TCPP@GQD NT in the presence (+) or absence (−) of RGD ($n = 3$, $^{**}p < 0.01$). f) Ex vivo FL images of tumor tissues and g) fluorescence intensity measurements of stromal (ST) and tumor (T). A549 tumor-bearing mice were intravenously injected with TCPP@GQD NT or TCPP@GQD.

tumor tissue section directly showed that the TCPP@GQD NT accumulated in lysosome at 4 h postinjection (p.i.), and further disassembled into small pieces at 24 h p.i. (Figure S30, Supporting Information). Then, the feasibility of in vivo imaging was evaluated by performing fluorescence and magnetic resonance duplex imaging. As shown in **Figure 3**a, the fluorescence signal increased in the tumor area with time and reached the plateau at 24 h p.i. Afterward, the fluorescence signal gradually decreased over time. Interestingly, the fluorescence signal of TCPP@GQD NT could be detected in the tumor area even at 96 h p.i. (Figure S31, Supporting Information). The long tumor retention time benefits for repeated PDT with only one injection. Notably, an increased fluorescence signal of tumor area was observed at 24 h p.i., while the fluorescence signal from the TCPP@GQD NT in tube remained stably. The ex vivo fluorescence images at different time points after i.v. injection indicated that TCPP@GQD NT was mainly metabolized by the liver (Figure S32a, Supporting Information). Blood circulation behavior of TCPP@GQD NT suggested that the metabolic half-life time of the TCPP@GQD NT was 7.8 h (Figure S32b, Supporting Information).

TCPP usually adopts as a planar chelate form to accept metal ions.[26] Some of the metal-chelates, such as Mn-TCPP and Gd-TCPP, have been explored as MRI contrast agents because the chelating paramagnetic metals can promote the relaxivity of water. In this work, the solubility of Mn-TCPP was significantly improved after loading by GQD NT. The as-prepared

Mn-TCPP@GQD NT showed good dispersity in aqueous solution. The T_1-weighted MR images revealed that the tumor contrast was obviously enhanced at 24 h p.i. (Figure 3b), and the longitudinal relaxation time of tumor tissues decreased from 2.7 to 1.9 s. The fluorescence signal and MRI SNR of tumors showed the similar pattern (Figure 3c), indicating the high tumor accumulation of TCPP@GQD NT or Mn-TCPP@GQD NT after i.v. injection. Due to the slow transformation of GQD NT that triggered by tumor acidic microenvironment, the encapsulated TCPP/Mn-TCPP could be released gradually in tumor tissues, their fluorescence or magnetic resonance signals gradually increased and maintained for several days.

The RGD active-targeting behavior of GQD NT was also investigated. The ex vivo FLI (Figure 3d) and quantitative analysis (Figure 3e) showed that tumor tissues exhibited high fluorescence signal. Notably, the fluorescence signal of tumor tissue was higher in the present of RGD than that group without RGD. Quantitative analysis (Figure 3e and Figure S33, Supporting Information) demonstrated that the fluorescence intensity of tumor tissues in RGD (+) group was 1.3 times higher than that of RGD (−) group. All these results illustrated the high tumor accumulation of TCPP@GQD NT or Mn-TCPP@GQD NT after i.v. injection, and RGD modification further improved the tumor accumulation of GQD NT.

The tumor sections were further studied to confirm the in vivo penetration ability of TCPP@GQD NT. As shown in Figure 3f, the present of yellow fluorescent indicated that TCPP was successfully delivered to tumor tissues. At the same PSs dose, the fluorescence intensity of mice injected with TCPP@GQD NT was 2.5 times higher than that of mice injected with TCPP@GQD. Notably, the fluorescence signal of tumor site accounted for 42% of the whole tumor tissue (including the parenchyma and peripheral regions of tumor) in TCPP@GQD NT injected mice (Figure 3g), which was comparable to that of TCPP@GQD injected mice (39%). Thus, the PS delivered by the designed GQD NT could distribute deeply in the tumor parenchyma like drugs transported by small-sized GQD. These results demonstrated that the designed nanotransformers not only improved the targeting ability, but also facilitated the PSs penetration in tumors.

In this work, subcutaneous A549 tumor-bearing mice model was used for biodistribution studies of TCPP@GQD NT through i.v. injection. In the future, orthotopic lung tumor-bearing mice model will be used. Due to the different location of tumors, the administration method of TCPP@GQD NT should be considered carefully. Compared with i.v. injection, spray administration may further increase the accessibility and accumulation of TCPP@GQD NT in orthotopic lung tumor tissues.[27] More efforts should be devoted to the evaluation of TCPP@GQD NT on different animal models.

2.5. In Vivo Antitumor Treatment of TCPP@GQD NT

Encouraged by the high tumor accumulation of TCPP@GQD NT, we further evaluated the in vivo PDT efficiency on A549 tumor-bearing mice. In detail, mice were intravenously administered with saline, GQD NT, or TCPP@GQD NT, respectively. The 650 nm laser irradiation is fixed at the dose of 100 mW cm^{-2} for 10 min every time. For TCPP@GQD NT plus laser irradiation group, we implemented a treatment plan of one i.v. injection plus four times of laser irradiation (**Figure 4**a). The body weight in all groups were stable during the treatments (Figure 4b). Mice in the repeated PDT treatment groups showed the highest survival rate (Figure 4c). As shown in Figure 4d, tumors in the saline plus laser group and GQD NT plus laser group showed similar growth trend as those in saline group. Meanwhile, TCPP@GQD NT cannot inhibit the tumor growth without laser irradiation. In comparison, mice treated with TCPP@GQD NT plus laser irradiation showed obvious tumor growth inhibition. At the end of treatment, tumor growth in TCPP@GQD NT plus laser irradiation groups was significantly inhibited (Figure 4e). Meanwhile, tumors in other four groups were enormously enlarged (Figure S34, Supporting Information). Interestingly, the repeated PDT with twice injection could almost completely ablated the tumors, four of five tumors were completely eliminated. Significantly, the total injection dose for tumor ablation was reduced to 3.5 μmol kg^{-1}, which was 10–30 times lower than that of the reported PDT strategies (Table S2, Supporting Information), indicating the high antitumor efficiency of repeated PDT based on TCPP@GQD NT.

As shown in Figure 4f, the hematoxylin and eosin (H&E) staining images showed obvious shrinking of nuclei in TCPP@GQD NT plus laser irradiation groups, revealing the typical necrosis/apoptosis of tumor cells. This result was further confirmed by the significant increase in the number of TUNEL positive nuclei. The expression of Ki-67 is closely related to mitosis, and has been used as an indicator to reveal cell proliferation. Clearly, TCPP@GQD NT plus laser group showed the down-regulation of Ki-67 expression, revealing that cell proliferation was strongly inhibited. One can see that cell apoptosis and proliferation inhibition of the repeated PDT with twice injection group were higher than one injection group. In short, TCPP@GQD NT induced repeatable PDT could effectively trigger the tumor cell apoptosis and inhibit their proliferation.

The in vivo biocompatibility of TCPP@GQD NT was also evaluated. No detectable pathological changes in major organs were observed in TCPP@GQD NT treated groups (Figure S35, Supporting Information), indicating that the TCPP@GQD NT had good biocompatibility. Blood routine examination and blood biochemistry assays also indicated that TCPP@GQD NT had little effect on liver function, kidney function and other physiological indexes (Figures S36–S38, Supporting Information). The above results demonstrated the good biocompatibility of TCPP@GQD NT.

3. Conclusions

In this study, we exploited a tumor acidity-triggered transformation nanovehicle to overcome the overdose challenges in PDT. During the self-assembly process between the loading, linking and targeting modules, MRI contrast agent Mn-TCPP and PS TCPP were simultaneously encapsulated and protected by the surrounding GQD and PEG, resulting in increased loading efficacy and retained drug activity. Upon reaching tumor, the vehicle GQD NT could "recognize" the acidic microenvironment, and transformed into a loose state with the diameter enlarged to ≈100 nm for longer tumor retention. Moreover, the slight

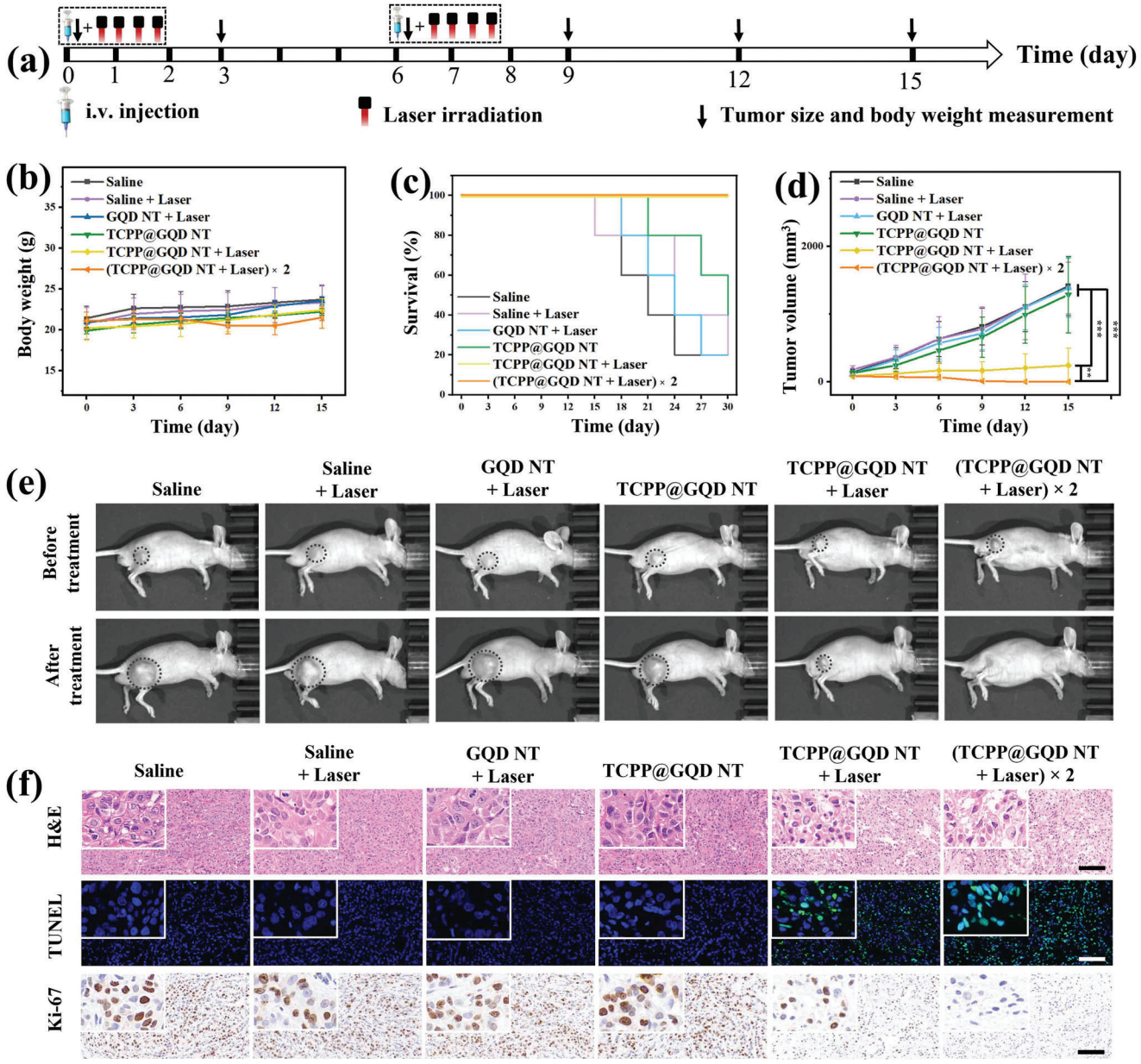

Figure 4. In vivo repeated PDT. a) Diagrammatic representation of therapeutic experiments. b) Body weight changes of A549 tumor-bearing mice in different treatment groups. c) Survival curves of A549 tumor-bearing mice after treatments. d) Tumor growth curves of A549 tumor-bearing mice treated with saline, GQD NT, TCPP/GQD NT with or without laser irradiation ($n = 5$, mean ± s.d., $^{**}p < 0.01$, $^{***}p < 0.001$). e) Photographs of A549 tumor-bearing mice before and after treatments. Tumor area is circled with grey dashed line. f) Representative H&E, TUNEL and Ki-67 staining images of tumor tissue sections of mice with various treatments. Scale bar, 100 μm.

photothermal effect of GQD NT improved the permeability of cancer cells and further enhanced the accumulation of the nanocomposite in tumor areas. The transformed GQD NT further disassembled and released the encapsulated drugs, which "turned-on" the FLI/MRI signals and activated the subsequent PDT treatment under light irradiation. Due to the efficient targeting and long retention time in tumors, the GQD NT encapsulated drugs largely aggregated in target areas, resulting high contrast in dual-modal imaging of tumor tissues. More importantly, the long tumor retention of the transported TCPP over 96 h provided a long period for PDT treatment. A treatment plan, one injection followed by 4 times of laser irradiation, was designed for effective PDT. Tumor growth was greatly inhibited, four of five tumors were ablated after the repeated PDT with twice injection. Notably, the introduced GQD NT decreased the total PS dose to a very low level at 3.5 μmol kg^{-1}, which was expected to overcome the overdose problems in repeated PDT. In a word, the designed nanotransformer provided an intelligent vehicle for next generation nanotherapeutics, exploiting a promising approach for long-time tumor imaging and efficient treatment.

Supporting Information

Supporting Information is available from the Wiley Online Library or from the author.

Acknowledgements

Y.Y. and B.W. contributed equally to this work. This work was supported by National Key R&D Program of China (2018YFA0704000), National Natural Science Foundation of China (82127802, 22274162, 81871453, 21921004), Key Research Program of Frontier Sciences, CAS (ZDBS-LY-JSC004), the Scientific Instrument Developing Project of the Chinese Academy of Sciences (GJJSTD20200002), Hubei Provincial Key Technology Foundation of China (2021ACA013), and Shenzhen Science and Technology Program (KQTD20190929172538530).X.Z. acknowledges the support from the Tencent Foundation through the XPLORER PRIZE. Y.Y. acknowledges the support from the Youth Innovation Promotion Association, CAS (2022336).

Conflict of Interest

The authors declare no conflict of interest.

Data Availability Statement

Research data are not shared.

Keywords

fluorescence imaging, graphene quantum dots, magnetic resonance imaging, photodynamic therapy, self-assembly

Received: December 4, 2022
Revised: March 6, 2023
Published online: April 25, 2023

[1] a) R. van der Meel, E. Sulheim, Y. Shi, F. Kiessling, W. J. M. Mulder, T. Lammers, *Nat. Nanotechnol.* **2019**, *14*, 1007. b) S. Lei, J. Zhang, N. T. Blum, M. Li, D. Y. Zhang, W. Yin, F. Zhao, J. Lin, P. Huang, *Nat. Commun.* **2022**, *13*, 1298. c) W. Fan, B. Yung, P. Huang, X. Chen, *Chem. Rev.* **2017**, *117*, 13566. d) T. Lammers, *Nat. Mater.* **2020**, *19*, 1257. e) Y. Zhang, S. Bo, T. Feng, X. Qin, Y. Wan, S. Jiang, C. Li, J. Lin, T. Wang, X. Zhou, Z. Jiang, P. Huang, *Adv. Mater.* **2019**, *31*, 1806444.

[2] a) Y. Wang, Y. Deng, H. Luo, A. Zhu, H. Ke, H. Yang, H. Chen, *ACS Nano* **2017**, *11*, 12134. b) Q. Chen, J. Chen, Z. Yang, J. Xu, L. Xu, C. Liang, X. Han, Z. Liu, *Adv. Mater.* **2019**, *31*, 1802228. c) J. Liu, M. Wu, Y. Pan, Y. Duan, Z. Dong, Y. Chao, Z. Liu, B. Liu, *Adv. Funct. Mater.* **2020**, *30*, 1908865. d) Y. M. Zhang, Y. H. Liu, Y. Liu, *Adv. Mater.* **2020**, *32*, 1806158. e) X. Chen, S. Lei, J. Lin, P. Huang, *Expert Opin. Drug Delivery* **2022**, *19*, 1487. f) H. Huang, J. F. Lovell, *Adv. Funct. Mater.* **2017**, *27*, 1603524.

[3] a) B. Liu, X. Luo, B. Deng, J. Wang, D. W. McComb, Y. Shi, K. M. L. Gaensler, X. Tan, A. L. Dunn, B. A. Kerlin, Y. Dong, *Nano Lett.* **2015**, *15*, 8099. b) F. Liu, N. Ding, D. Huo, G. Yang, K. Wei, G. Guan, Y. Li, J. Yang, T. Wang, Y. Wang, J. Tan, W. Zeng, C. Zhu, *Adv. Healthcare Mater.* **2019**, *8*, 1900386. c) M. M. Billingsley, A. G. Hamilton, D. Mai, S. K. Patel, K. L. Swingle, N. C. Sheppard, C. H. June, M. J. Mitchell, *Nano Lett.* **2022**, *22*, 533.

[4] a) S. Zhang, C. Chen, C. Xue, D. Chang, H. Xu, B. J. Salena, Y. Li, Z. S. Wu, *Angew. Chem., Int. Ed.* **2020**, *59*, 14584. b) A. Harguindey, D. W. Domaille, B. D. Fairbanks, J. Wagner, C. N. Bowman, J. N. Cha, *Adv. Mater.* **2017**, *29*, 1700743. c) D. A. Estabrook, R. A. Day, E. M. Sletten, *Angew. Chem., Int. Ed.* **2021**, *60*, 17362.

[5] a) S. Tan, H. Yang, S. Xue, J. Qiao, M. Salarian, K. Hekmatyar, Y. Meng, R. Mukkavilli, F. Pu, O. Y. Odubade, W. Harris, Y. Hai, M. L. Yushak, V. M. Morales-Tirado, P. Mittal, P. Z. Sun, D. Lawson, H. E. Grossniklaus, J. J. Yang, *Sci. Adv.* **2020**, *6*, eaav7504. b) S. Xue, H. Yang, J. Qiao, F. Pu, J. Jiang, K. Hubbard, K. Hekmatyar, J. Langley, M. Salarian, R. C. Long, R. G. Bryant, X. P. Hu, H. E. Grossniklaus, Z. R. Liu, J. J. Yang, *Proc. Natl. Acad. Sci USA* **2015**, *112*, 6607. c) H. R. Jia, Y. X. Zhu, X. Liu, G. Y. Pan, G. Gao, W. Sun, X. Zhang, Y. W. Jiang, F. G. Wu, *ACS Nano* **2019**, *13*, 11781.

[6] a) R. K. Jain, T. Stylianopoulos, *Nat. Rev. Clin. Oncol.* **2010**, *7*, 653. b) J. Fang, H. Nakamura, H. Maeda, *Adv. Drug Delivery Rev.* **2011**, *63*, 136. c) Y. Dai, C. Xu, X. Sun, X. Chen, *Chem. Soc. Rev.* **2017**, *46*, 3830. d) J. K. Tee, L. X. Yip, E. S. Tan, S. Santitewagun, A. Prasath, P. C. Ke, H. K. Ho, D. T. Leong, *Chem. Soc. Rev.* **2019**, *48*, 5381. e) S. Wang, P. Huang, X. Chen, *Adv. Mater.* **2016**, *28*, 7340.

[7] a) R. H. Fang, A. V. Kroll, W. Gao, L. Zhang, *Adv. Mater.* **2018**, *30*, 1706759. b) C. Chu, J. Yu, E. Ren, S. Ou, Y. Zhang, Y. Wu, H. Wu, Y. Zhang, J. Zhu, Q. Dai, X. Wang, Q. Zhao, W. Li, Z. Liu, X. Chen, G. Liu, *Adv. Sci.* **2020**, *7*, 2000346. c) M. Izci, C. Maksoudian, B. B. Manshian, S. J. Soenen, *Chem. Rev.* **2021**, *121*, 1746.

[8] a) K. N. Sugahara, T. Teesalu, P. P. Karmali, V. R. Kotamraju, L. Agemy, O. M. Girard, D. Hanahan, R. F. Mattrey, E. Ruoslahti, *Cancer Cell* **2009**, *16*, 510. b) Z. Liang, Q. Wang, H. Liao, M. Zhao, J. Lee, C. Yang, F. Li, D. Ling, *Nat. Commun.* **2021**, *12*, 3840. c) T. He, J. He, M. R. Younis, N. T. Blum, S. Lei, Y. Zhang, P. Huang, J. Lin, *ACS Appl. Mater. Interfaces* **2021**, *13*, 22204.

[9] a) J. Liu, M. Li, Z. Luo, L. Dai, X. Guo, K. Cai, *Nano Today* **2017**, *15*, 56. b) S. Wang, P. Huang, X. Chen, *ACS Nano* **2016**, *10*, 2991. c) H. L. Chee, C. R. R. Gan, M. Ng, L. Low, D. G. Fernig, K. K. Bhakoo, D. Paramelle, *ACS Nano* **2018**, *12*, 6480.

[10] a) T. Shi, W. Sun, R. Qin, D. Li, Y. Feng, L. Chen, G. Liu, X. Chen, H. Chen, *Adv. Funct. Mater.* **2020**, *30*, 2001166. b) H. Chen, Y. Qiu, D. Ding, H. Lin, W. Sun, G. D. Wang, W. Huang, W. Zhang, D. Lee, G. Liu, J. Xie, X. Chen, *Adv. Mater.* **2018**, *30*, 1802748. c) Z. Li, S. Li, Y. Guo, C. Yuan, X. Yan, K. S. Schanze, *ACS Nano* **2021**, *15*, 4979. d) H. Zhang, K. Liu, S. Li, X. Xin, S. Yuan, G. Ma, X. Yan, *ACS Nano* **2018**, *12*, 8266. e) B. M. Ludy, C. D. Walsh, G. Zheng, *Angew. Chem., Int. Ed.* **2019**, *58*, 2558.

[11] a) S. B. Brown, E. A. Brown, I. Walker, *Lancet Oncol.* **2004**, *5*, 497. b) J. Webber, M. Herman, D. Kessel, D. Fromm, *Ann. Surg.* **1999**, *230*, 12.

[12] S. S. Lucky, K. C. Soo, Y. Zhang, *Chem. Rev.* **2015**, *115*, 1990.

[13] a) J. Chen, Y. Zhu, S. Kaskel, *Angew. Chem., Int. Ed.* **2021**, *60*, 5010. b) Q. Deng, P. Sun, L. Zhang, Z. Liu, H. Wang, J. Ren, X. Qu, *Adv. Funct. Mater.* **2019**, *29*, 1903018. c) J. Y. Zeng, M. Z. Zou, M. Zhang, X. S. Wang, X. Zeng, H. Cong, X. Z. Zhang, *ACS Nano* **2018**, *12*, 4630.

[14] a) J. F. Lovell, C. S. Jin, E. Huynh, H. Jin, C. Kim, J. L. Rubinstein, W. C. W. Chan, W. Cao, L. V. Wang, G. Zheng, *Nat. Mater.* **2011**, *10*, 324. b) Y. Sun, Y. Zhang, Y. Gao, P. Wang, G. He, N. T. Blum, J. Lin, Q. Liu, X. Wang, P. Huang, *Adv. Mater.* **2020**, *32*, 2004481. c) J. F. Lovell, C. S. Jin, E. Huynh, T. D. MacDonald, W. Cao, G. Zheng, *Angew. Chem., Int. Ed.* **2012**, *51*, 2429.

[15] a) H. J. Cho, S. J. Park, W. H. Jung, Y. Cho, D. J. Ahn, Y. S. Lee, S. Kim, *ACS Nano* **2020**, *14*, 15793. b) Y. Deng, W. Zhan, G. Liang, *Adv. Healthcare Mater.* **2021**, *10*, 2001211.

[16] a) L. Li, C. Shao, T. Liu, Z. Chao, H. Chen, F. Xiao, H. He, Z. Wei, Y. Zhu, H. Wang, X. Zhang, Y. Wen, B. Yang, F. He, L. Tian, *Adv. Mater.* **2020**, *32*, 2003471. b) P. Zhang, J. Wang, H. Chen, L. Zhao, B. Chen, C. Chu, H. Liu, Z. Qin, J. Liu, Y. Tan, X. Chen, G. Liu, *J. Am. Chem. Soc.* **2018**, *140*, 14980. c) Z. Guo, H. He, Y. Zhang, J. Rao, T. Yang, T. Li, L. Wang, M. Shi, M. Wang, S. Qiu, X. Song, H. Ke, H. Chen, *Adv. Mater.* **2021**, *33*, 2004225. d) D. Chen, Q. Tang, J. Zou, X. Yang, W. Huang, Q. Zhang, J. Shao, X. Dong, *Adv. Healthcare Mater.* **2018**, *7*, 1701272.

[17] a) Y. Wang, W. Wu, J. Liu, P. N. Manghnani, F. Hu, D. Ma, C. Teh, B. Wang, B. Liu, *ACS Nano* **2019**, *13*, 6879. b) M. X. Wu, Y. W. Yang, *Adv. Mater.* **2017**, *29*, 1606134.

[18] a) R. Xing, Q. Zou, C. Yuan, L. Zhao, R. Chang, X. Yan, *Adv. Mater.* **2019**, *31*, 1900822. b) R. Chang, Q. Zou, L. Zhao, Y. Liu, R. Xing, X. Yan, *Adv. Mater.* **2022**, *34*, 2200139.

[19] a) B. C. Thompson, E. Murray, G. G. Wallace, *Adv. Mater.* **2015**, *27*, 7563. b) C. Nie, L. Ma, S. Li, X. Fan, Y. Yang, C. Cheng, W. Zhao, C. Zhao, *Nano Today* **2019**, *26*, 57. c) S. Chung, R. A. Revia, M. Zhang, *Adv. Mater.* **2021**, *33*, 1904362. d) J. Lin, X. Chen, P. Huang, *Adv. Drug Delivery Rev.* **2016**, *105*, 242. e) P. Huang, C. Xu, J. Lin, C. Wang, X. Wang, C. Zhang, X. Zhou, S. Guo, D. Cui, *Theranostics* **2011**, *1*, 240. f) X. T. Zheng, A. Ananthanarayanan, K. Q. Luo, P. Chen, *Small* **2015**, *11*, 1620.

[20] a) C. Xu, H. Hong, Y. Lee, K. S. Park, M. Sun, T. Wang, M. E. Aikins, Y. Xu, J. J. Moon, *ACS Nano* **2020**, *14*, 13268. b) L. Cheng, X. Wang, F. Gong, T. Liu, Z. Liu, *Adv. Mater.* **2020**, *32*, 1902333.

[21] a) Y. Yang, A. M. Asiri, Z. Tang, D. Du, Y. Lin, *Mater. Today* **2013**, *16*, 365. b) Y. Yan, J. Gong, J. Chen, Z. Zeng, W. Huang, K. Pu, J. Liu, P. Chen, *Adv. Mater.* **2019**, *31*, 1808283. c) Y. Yang, S. Chen, H. Li, Y. Yuan, Z. Zhang, J. Xie, D. W. Hwang, A. Zhang, M. Liu, X. Zhou, *Nano Lett.* **2019**, *19*, 441.

[22] a) J. Ge, M. Lan, B. Zhou, W. Liu, L. Guo, H. Wang, Q. Jia, G. Niu, X. Huang, H. Zhou, X. Meng, P. Wang, C. S. Lee, W. Zhang, X. Han, *Nat. Commun.* **2014**, *5*, 4596. b) Y. Chong, Y. Ma, H. Shen, X. Tu, X. Zhou, J. Xu, J. Dai, S. Fan, Z. Zhang, *Biomaterials* **2014**, *35*, 5041. c) W. Du, Y. Chong, X. Hu, Y. Wang, Y. Zhu, J. Chen, X. Li, Q. Zhang, G. Wang, J. Jiang, G. Liang, *Adv. Funct. Mater.* **2020**, *30*, 1908073. d) M. R. Younis, G. He, J. Lin, P. Huang, *Front Chem.* **2020**, *8*, 424. e) A. Ghaffarkhah, E. Hosseini, M. Kamkar, A. A. Sehat, S. Dordanihaghighi, A. Allahbakhsh, C. van der Kuur, M. Arjmand, *Small* **2022**, *18*, 2102683.

[23] a) H. Wang, K. J. Chen, S. Wang, M. Ohashi, K. Kamei, J. Sun, J. H. Ha, K. Liu, H. R. Tseng, *Chem. Commun.* **2010**, *46*, 1851. b) S. Wang, K. J. Chen, T. H. Wu, H. Wang, W. Y. Lin, M. Ohashi, P. Y. Chiou, H. R. Tseng, *Angew. Chem., Int. Ed.* **2010**, *49*, 3777. c) L. Wang, L. Li, Y. Fan, H. Wang, *Adv. Mater.* **2013**, *25*, 3888. d) Q. D. Hu, G. P. Tang, P. K. Chu, *Acc. Chem. Res.* **2014**, *47*, 2017.

[24] a) M. Li, D. Xie, X. Tang, C. Yang, Y. Shen, H. Zhou, W. Deng, J. Liu, S. Cai, L. Bai, Y. Wang, *Nano Lett.* **2021**, *21*, 6304. b) Q. Chen, Q. Hu, E. Dukhovlinova, G. Chen, S. Ahn, C. Wang, E. A. Ogunnaike, F. S. Ligler, G. Dotti, Z. Gu, *Adv. Mater.* **2019**, *31*, 1970166. c) T. Feng, L. Zhou, Z. Wang, C. Li, Y. Zhang, J. Lin, D. Lu, P. Huang, *Biomaterials* **2020**, *232*, 119709. d) Y. W. Bao, X. W. Hua, X. Chen, F. G. Wu, *Biomaterials* **2018**, *183*, 30. e) G. Gao, Y. W. Jiang, H. R. Jia, W. Sun, Y. Guo, X. W. Yu, X. Liu, F. G. Wu, *Biomaterials* **2019**, *223*, 119443.

[25] a) Y. Li, J. Yang, G. Gu, X. Guo, C. He, J. Sun, H. Zou, H. Wang, S. Liu, S. Zhang, K. Wang, L. Yang, Y. Jiang, L. Wu, X. Sun, *Nano Lett.* **2022**, *22*, 963. b) H. J. Li, J. Z. Du, X. J. Du, C. F. Xu, C. Y. Sun, H. X. Wang, Z. T. Cao, X. Z. Yang, Y. H. Zhu, S. Nie, J. Wang, *Proc. Natl. Acad. Sci USA* **2016**, *113*, 4164. c) V. P. Chauhan, T. Stylianopoulos, J. D. Martin, Z. Popović, O. Chen, W. S. Kamoun, M. G. Bawendi, D. Fukumura, R. K. Jain, *Nat. Nanotechnol.* **2012**, *7*, 383. d) Z. Popović, W. Liu, V. P. Chauhan, J. Lee, C. Wong, A. B. Greytak, N. Insin, D. G. Nocera, D. Fukumura, R. K. Jain, M. G. Bawendi, *Angew. Chem., Int. Ed.* **2010**, *49*, 8649.

[26] Y. Ding, W. H. Zhu, Y. Xie, *Chem. Rev.* **2017**, *117*, 2203.

[27] S. Ma, Z. Cong, J. Wei, W. Chen, D. Ge, F. Yang, Y. Liao, *J. Controlled Release* **2022**, *350*, 132.